Thermodynamic difficulties to determine a critical chloride threshold for breakdown of the protective layer of steel reinforcement in a maritime concrete structure

Anthony Soive, Stéphanie Bonnet, Abdelhafid Khelidj, Véronique Baroghel-Bouny

Thermodynamic difficulties to determine a critical chloride threshold for breakdown of the protective layer of steel reinforcement in a maritime concrete structure

Anthony Soive[a], Stéphanie Bonnet[b]*, Abdelhafid Khelidj[b] and Véronique Baroghel-Bouny[c]

[a]*Cerema, GeoCoD research Team, Aix-en-Provence, France;* [b]*Institut de Recherche en Génie Civil et Mécanique (GeM), I.U.T., Département Génie Civil, Université de Nantes, Saint-Nazaire, France;* [c]*FM2D Laboratory, Materials and Structures Department, Université Gustave Eiffel, Champs-sur-Marne, France*

There is much debate on the expression used for the critical chloride threshold as well as on its value for breakdown of the protective layer of steel for reinforced concrete. In fact, this concept suggests that the breakdown is only driven by dissolution of the protective layer. A reactive transport model including dissolution and precipitation of solid species with their kinetics is then used in order to simulate the ingress deleterious substances in a concrete exposed to seawater and the chemical degradation of the oxides and hydroxides present in the protective layers covering a steel rebar. The numerical results confirm that most of the oxides are thermodynamically very stable even after a long period of exposure, especially in the inner layer. This finding suggests that corrosion initiation depends on protective layer thickness and history. These results also provide a sound explanation why a wide scatter of values of critical chloride threshold values is reported in literature.

Keywords: Reinforced concrete; chloride; protective layer; dissolution threshold

1. Introduction

Chloride-induced corrosion of steel reinforcement is one of the main causes of premature deterioration of marine concrete structures. Therefore this deterioration mechanism is considered an essential factor to be examined in more detail in order to better understand the long-term behavior of materials used to build and repair concrete structures. One of the critical points is the breakdown of the protective layer covering steel reinforcement which, once it has happened, allows steel to corrode. However, this phenomenon is still unclear although essential in quantifying the service life of structures (Refs. [1, 2] to cite a few).

According to the literature, the protective layer breakdown in concrete corresponds to a critical concentration of chloride, this latter term being expressed as" critical chloride threshold" today. Generally, this threshold level at the depth of the reinforcement can be expressed in four ways: the concentration of total chlorides [3, 4], the concentration of free chlorides [5], the ratio $[Cl^-]/[OH^-]$ [6, 7] and the ratio $[Cl^-]/[ANC]$ [8]. In the last case, *ANC* is the neutralization capacity of an acid (or alkalinity), defined as follows: $[ANC] = 2[CO_3{}^{2-}] + [HCO_3{}^-] + [OH^-] - [H^+]$. Angst *et al.* [1] have listed the most influential parameters on breakdown among which steel-concrete interface, pH value of the pore solution and electrochemical potential of steel can be found. Cao *et al.* confirm that there is a wide scatter in critical chloride concentration (over 2 orders of magnitude) on a compilation of a significant number of data reported in Chinese publications [2]. The threshold level also depends on rebar surface conditions [9–11], properties of the rebar concrete interface [12] and chemistry of the concrete pore solution [8, 13–16]. Furthermore, the expression to be used for these thresholds is the subject of much debate. Ann *et al.* [17] and Glass *et al.* [8] show that the concentration of total chlorides is more relevant than the concentration of free chlorides or than the ratio $[Cl^-]/[OH^-]$. Hausmann [6] and Diamond [18] consider that the threshold level when expressed by the ratio $[Cl^-]/[OH^-]$ is constant regardless of the cement composition and concrete mix-design. Gouda [7] proposed the expression $[Cl^-]^{0.83}/[OH^-]$. However, other studies indicate that the threshold vary depending on the physico-chemical parameters close to the protective layer. For example, Li *et al.* [10] and Moreno *et al.* [19] show that the threshold level expressed as the ratio $[Cl^-]/[OH^-]$ increases when the *pH* increases. Yu *et al.* show also that corrosion depends on load-induced damage or casting-induced damage [20].

In the literature several theories have been proposed to explain the steel protective layer breakdown in an aggressive electrolyte solution. It was first considered, in 1964 by Kolotyrkin, as a physical adsorption mechanism [21]. Kolotyrkin reasoned that the adsorption of aggressive anions on the external surface of the protective layer increases the transfer of cations Fe^{2+}, Fe^{+3} to the surrounding electrolyte solution. Later, Dabosi *et al.* [22] corrected this Kolotrin's opinion by measuring only the Fe^{2+}-ions when bare steel is in contact with the electrolyte at a point where the protective layer has fractured. Dabosi *et al.* further proposed that the protective layer becomes thinner over the time due to gradual dissolution of its constituents until possibly complete dissolution occurs during intense local dissolution. The penetration mechanism proposed by Hoar *et al.* in 1965 [23] is very different from

*Corresponding author. Email: Stéphanie Bonnet Stephanie.Bonnet@univ-nantes.fr

the theory of Kolotyrkin since they consider only the transport of aggressive agents through the protective layer to reach the "iron/protective layer" interface, a zone in which these agents are most active (see Figure 1). The iron is then in direct contact with the aggressive agents. Iron dissolves as iron(II) ions which, themselves react with the hydroxide ions OH^-. The combination of these ions produces iron hydroxide $Fe(OH)_2$, which can then further react with other ions to form other oxides/hydroxides. These products finally precipitate at the "iron/protective layer" interface. As the molar volumes of the substances formed are larger than the original volume, this results into pressure creating stresses in the protective layer that may cause it to crack. In 1970, Vetter *et al.* [24] proposed a mechanism fairly similar to the one described previously. Nevertheless, Vetter *et al.* made the assumption that the protective layer has been previously damaged and already demonstrates micro-cracks. Propagation of aggressive agents through these cracks is then easier. Corrosion products resulting from the reactions of the aggressive agents with the" healthy" iron also lead to mechanical deterioration of the protective layer. In 1976 Strehblow [25] did not see these different mechanisms as being as contradicting. Quite the reverse: for Strehblow depassivation is characterized by three main mechanisms: (1) adsorption mechanism (physical and chemical), (2) mechanism involving penetration of aggressive agents through the protective layer, (3) mechanism involving failure of the layer due to formation of corrosion products formation in the iron/protective layer interface. All three of these mechanisms can occur simultaneously during the deterioration process. In addition, the phenomena associated with any of these mechanisms may influence the others.

In the scenarios previously described, only one scenario considers a dissolution of the protective layer by aggressive agents. The other scenarios involve a transport mechanism either through the protective layer or through micro-cracks. For all scenarios, the time to corrosion is then dependent on the steel-concrete interface and in particular the thickness of the protective layer [26] or to the mechanical history of the rebar (e.g. stress during rebar transport or casting, stress during service life of reinforced concrete). In the case of reinforced concrete, except at considering that for each reinforcement bar the protective layer thickness is similar or that micro-cracks always occurs at the same time, the scenarios other than dissolution should lead to a scatter of the critical chloride threshold value for the same cementitious material when exposed to the same environment but with different reinforcing bar. Although this scatter should then also be observed with the same reinforced concrete if the protective layer thickness varies along the reinforcing bar. Whereas all scenarios except one are dependent on depth or mechanical protective layer history, the concept of a critical chloride threshold suggests that the degradation of the protective layer is only driven by dissolution. Of course, ingress through the protective layer depends on a concentration gradient of the agressive agents but, once again, the time to reach the steel depends on the protective layer geometry (thickness) or mechanical history.

Faced with these different scenarios, there is a need to find out whether thermochemical reactions (dissolution) at the steel/concrete interface are sufficient on their own to explain the degradation phenomenon. Modeling should help to understand this protective layer degradation mechanism eventually affecting the steel used in reinforced concrete. A reactive transport model is then used in order to simulate the ingress of seawater in the concrete cover by taking into account the modification of hydrates and pore solution from the external concrete surface to the protective layer around the embedded steel and the chemical degradation of the oxides and hydroxides present in the protective layer covering a rebar. This numerical study focuses on the conditions of thermochemical (and kinetical) deterioration of the constituents of the protective layer in a concrete. The first part discusses what the concept of a critical chloride threshold implies. The second part describes the nature of the constituents of the protective layer and the reactive transport model. The third part presents simulation results and a discussion is proposed. Conclusions are presented in the final part.

2. Protective layer composition and corrosion products

Understanding the chemical deterioration mechanisms of the protective layer requires knowledge of its nature and its geometry. A electro-chemical balance between the interstitial solution and the reinforcement is set up, the reinforcement being "protected" by a protective layer and the alkalinity of the pore solution inside the concrete. In fact, this balance is an instable equilibrium since "healthy" steel is not present in natural conditions. Thus, corrosion of steel rebar is a slow process that cause the iron to oxidize and steel to have a protective layer of oxides and hydroxides on its external part. However, this process can be accelerated dramatically leading to protective layer breakdown.

In the highly alkaline environment present in concrete the nature of the protective layer on steel reinforcement has been examined in a number of studies [27–29]. According to the Pourbaix diagram [30], simplified for $25^{\circ}C$, two iron oxides in the protective layer are more stable when the iron is in contact with water, i.e. hematite and magnetite ($\alpha-Fe_2O_3$ and Fe_3O_4, respectively). In the protective layer also other iron oxides can be found, including hydrated oxides such as goethite, lepidocrocite and maghemite ($\alpha-FeOOH$, $\gamma-FeOOH$ and $\gamma-Fe_2O_3$, respectively) [27]. From a geometrical point of view, the protective layer is considered as a two-layered structure: an inner layer mainly composed of iron(II) oxides and an external layer mainly composed of iron(III) oxides [12, 29, 31–35] (see Figure 1). Suda *et al.* [36], Noda *et al.* [37] and Pan *et al.* [38] have experimentally determined that the outer layer of the protective layer in contact with the pore solution of the concrete cover is porous and consists of lepidocrocite $\gamma-FeOOH$ and goethite $\alpha-FeOOH$ or maghemite

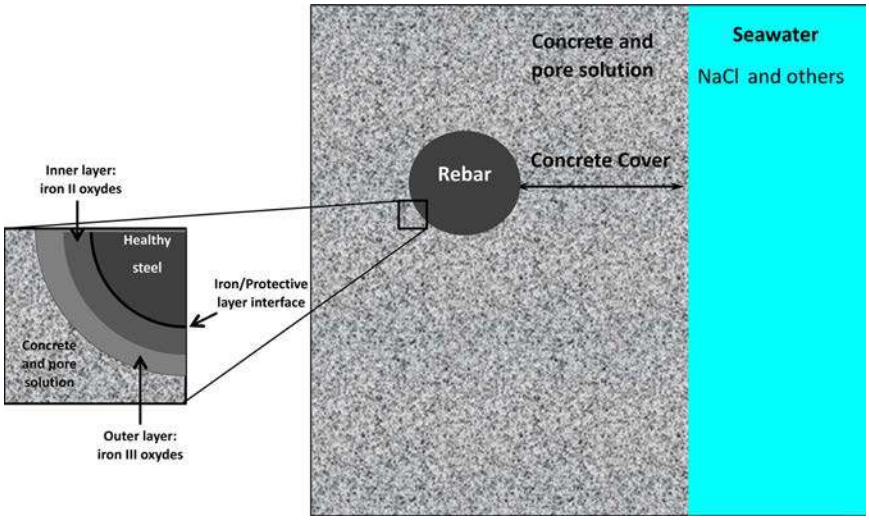

Figure 1. Reinforced concrete exposed to seawater and schematic protective layer on steel reinforcement as a two-layered structure.

$\gamma-Fe_2O_3$. The inner layer of the protective layer in contact with the" healthy" iron is denser than the outer layer and is made up of magnetite Fe_3O_4 and hematite $\alpha-Fe_2O_3$. In the literature the thicknesses of the protective layer is reported to be about 5 [28] to 10 nm [39–41] in an alkaline electrolyte solution.

When the ions contained in seawater enter the concrete, the electrochemical equilibrium is disturbed leading to precipitation of Friedel's salt, ettringite or dissolution of portlandite (to cite a few). Upon arrival of chloride ions, the equilibrium of the protective layer is also disturbed. The protective layer begins to deteriorate and reaction products may develop, such as akaganeite $(Fe(OH)_{2.7}Cl_{0.3})$ [42–45] and different forms of green rust, $Fe_4(OH)_8Cl \cdot nH_2O$ [46, 47], $Fe_6(OH)_{12}\ CO_3 \cdot 2H_2O$ [46, 48], $Fe_3O_2(OH)_4$, $Fe_8(OH)_{16}SO_3 \cdot 4H_2O$, $Fe_6(OH)_{12}SO_4 \cdot 2H_2O$ [49].

3. Numerical approach

3.1. Model description

In order to study the chemical dissolution of the protective layer components (oxide or hydroxide), a good estimation of the ionic concentrations close to the reinforcement is needed. To allow for a prediction of the ionic species ingress and the chemically consequences on oxides and hydroxides present in the protective layer, a physically and chemically based model is used. This model simulate the reactive transport of ionic species in the concrete cover and their possible reactions with the solid species as well as the dissolution of the protective layer oxides present arbitrarily at 3 cm depth. This model has been recently developed and validated in the case of the development of reaction products during chloride ingress in saturated concretes exposed to a chloride solution [50, 51] or to an external sulfate attack [52]. A simplified version of this model, assuming that adsorption of chloride on C-S-H depends linearly on chloride concentration, was also used to simulate chloride ingress in concrete subjected to wetting-drying cycles involving seawater in laboratory conditions during 1.5 years [53]. First, such a model is of interest to describe the evolution of the mineral phases and the composition of the ionic solution in time and space, especially close to a reinforcement bar. Second, it can help to estimate which conditions are required in order to dissolve the components of the protective layer.

The model used is based on mass transport and physico-chemical reactions. Diffusion is the main transport mechanism considered in this study. The equation for the submerged continually water-saturated conditions with coupling of transport processes to chemistry is as follows:

$$\frac{\partial \phi c_i}{\partial t} = \vec{\nabla}.\left(D_{e,i}\vec{\nabla}c_i\right) + q_i \tag{1}$$

where ϕ, c_i, D_e and q_i are the porosity [-], the ionic concentration $[mol.l^{-1}]$, the diffusion coefficient of ionic species i in the pore solution of the concrete $[m^2.s^{-1}]$ and a source term which describes ionic species that can either be physically bound or chemically react with the cementitious matrix $[mol.l^{-1}.s^{-1}]$, respectively.

Mineral dissolution/precipitation can modify the local porosity of the concrete. That is the reason why porosity is explicitly included in Equation 1. The magnitude of the effective diffusion coefficient can then be locally modified as it is expressed as a function of porosity as follows:

$$D_{e,i} = \tau\phi D_{wi} \tag{2}$$

where τ [-] is the tortuosity in the concrete and D_{wi} is the diffusion coefficient of species i in pure water.

The model only takes into account a common coefficient for both cationic, neutral and anionic species. The problem was simplified to a one-dimensional problem for the ingress of seawater in concrete. The chemical reactions were calculated assuming mineral precipitation/dissolution of the main concrete minerals with their kinetics during the transport process. They were calculated assuming thermodynamic equilibrium and kinetics for the

Table 1. Chemical and mineralogical composition of the binder (%) [55].

	SiO_2	Al_2O_3	Fe_2O_3	CaO	MgO	SO_3	K_2O	Na_2O	CO_2
CEMI	21.39	3.49	4.16	65.12	0.82	2.86	0.3	0.12	0.18
Fly ash	55.86	25.40	6.05	1.83	0.63	0.11	4.77	0.24	0.0

Table 2. Mix-design ($kg.m^{-3}$ of concrete), along with 90 day porosity accessible to water (measured after water curing) [55].

Concrete	Gravel/sand	Cement	Fly ash	Water	W/binder	Porosity
M30FA	986/879	223	95	166	0.52	0.141
M50	937/806	410	0	197	0.48	0.145

Table 3. Ionic composition of seawater from Atlantic Seawater at La Rochelle ($mol.l^{-1}$).

Na^+	Cl^-	K^+	Ca^{2+}	Mg^{2+}	$SO_4{}^{2-}$	$CO_3{}^{2-}$
0.459	0.546	9.71×10^{-3}	9.97×10^{-3}	5.22×10^{-2}	2.76×10^{-2}	2.029×10^{-3}
pH	8.1					

protective layer components. The kinetic laws used in this study follow the expression given by Lasaga *et al.* [54]:

$$r_n = \pm k_n A_{s,n} |1 - \Omega_n| \qquad n = 1, .., N_q \tag{3}$$

where positive values of r indicate dissolution and negative values precipitation of mineral species n, k is the rate constant ($mol.m^{-2}.s^{-1}$). A_s is the specific reactive surface area ($m^2.g^{-1}$), Ω is the mineral saturation ratio [-]. When the reaction approaches an equilibrium, Ω approximates 1, and the chemical reaction rate tends towards 0. q is the number of minerals under kinetic constraints.

Ionic species can also be adsorbed on C-S-H. The driving process for absorption can be expressed as follows:

$$K_{eq} = K \exp\left(\frac{-F\psi_0}{RT}\right) \tag{4}$$

where K_{eq}, K, F, ψ, R and T are the equivalent solubility product [-], the solubility product [-], the Faraday's constant [$C.mol^{-1}$] the surface potentiel [V], the ideal gaz constant [$J.K^{-1}.mol^{-1}$] and the temperature [K], respectively. In this work the surface potential is calculated by the Gouy-Chapman diffuse layer theory in this work.

3.2. Input data

Two binder compositions and concrete mix-designs were tested (see Tables 1 and 2). The first concrete contains fly ash (M30FA) whereas the second one is based on an ordinary Portland cement (M50). The Portland cement composition was the same for all concretes. The concretes were exposed to seawater during 19 years (see Table 3 for the seawater chemical composition). In the numerical study, the binders are considered to be very well hydrated. The initial mineral composition, calculated with the hydration model developed by Lavergne *et al.* [56] which is based on research by Dilnesa *et al.* [57], is given in Table 4.

In the simulations only fully water-saturated cementitious materials are considered. The calculations were performed in one dimension. A simple mesh composed of one 200-element row was used which represented 200 mm of RC structural elements (BHP2000 concretes) which are prisms with trapezoidal section (thickness equal to 400 mm at the base and 200 mm at the top. Only one measurement by period of exposure was done. The rebar itself has not been modelled. The volume fraction of each oxide and hydroxide and their distribution in the thickness of the protective layer is not well documented in the literature, especially in concrete. In addition, from a numerical point of view, modeling such a geometry can lead to serious numerical problems. Finally, one objective of this paper was to estimate the stability of each oxide and hydroxide in the presence of chloride ions in the vicinity of the steel/concrete interface. Thus, the choice that has been made was to add a cell at 3 cm depth in which a small volume fraction [-] of each oxide or hydroxides has been put (lepidocrocite, maghemite, goethite, hematite, magnetite). Then a simulation was done in order to identify the ability of each oxide and hydroxide to dissolve. The reactive transport code Toughreact [58] was used whereas the Thermoddem database was employed for most mineral species [59]. Information on missing mineral species ($C_3AS_{0.84}H_{4.32}$, $C_3FS_{1.34}H_{3.32}$, Kuzel's salt and Akaganeite) have been taken from other databases such as Cemdata18 [60] and added to the database used in this work according to the standard thermodynamic properties presented in Table 5. Simulations have been performed for a constant temperature ($25^\circ C$). Data on chemical reactions and solubility products of minerals species are provided in Table 6.

4. Numerical results

4.1. Chloride ingress

The study of the dissolution of the protective layer needs a good estimation of the ionic species at the level of the outer part of the reinforcement as a function of time. The proposed reactive transport model aims at providing such information. Figure 2 shows the calculated chloride concentration profiles for M30FA and M50 after 19 year-exposure to seawater. The numerical results are compared

Table 4. Initial mineralogy of the hydrated ordinary Portland cement considered in the calculations.

	Volume fraction of solid ($m^3.m^{-3}$)	
Mineral	M30FA	M50
C-S-H 1.6	–	5.4×10^{-2}
C-S-H 1.1	1.88×10^{-1}	1.2×10^{-1}
Monosulfate	2.2×10^{-2}	–
Ettringite	3.2×10^{-2}	2.9×10^{-2}
Portlandite	–	6.8×10^{-2}
Monocarbonate	1.6×10^{-2}	
Hydroandradite ($C_3FS_{1.34}H_{3.32}$)	3.8×10^{-3}	6.5×10^{-3}
Gypsum	–	4.4×10^{-3}
Calcite	–	3.8×10^{-3}

Table 5. Standard thermodynamic properties of iron oxides/hydroxides and ionic species at $25^{\circ}C$ and $1.1013 \times 10^5\,Pa$.

	$\triangle H^0_{T_0}$ $KJ\,/\,mol$	$S^0_{T_0}$ $J/(mol.K)$	Reference
Fe^{3+}	−49.00	−278.44	[61]
Fe^{2+}	−90.41	−107.10	[61]
H_2O	−285.83	69.95	[62]
H^+	0	0	Convention
OH^-	−230.01	−10.71	[63]
Cl^-	−167.08	56.60	[62]
$C_3FS_{1.34}H_{3.32}$	−4994	820	[60]
Kuzel's salt ($Ca_4Al_2(SO_4)_{0.5}Cl(OH)_{12}.6H_2O$)	−8472	820	[64]
Akaganeite ($Fe(OH)_{2.7}Cl_{0.3}$)	−842.125	91.5	[65,66]

to experimental data (one profile for each period of exposure) obtained from unreinforced concrete specimens (M30FA and M50) exposed to seawater and wetting-drying cycles (tidal zone) in the La Rochelle harbour [67]. The contribution of free chloride concentration, chlorides adsorbed on C-S-H, chlorides bound in Friedel's and Kuzel's salt and the sum of all (total chloride) are presented. Diffusion coefficients of all ionic species in M30FA and M50 are $6.35\,10^{-12}$ and $5.55\,10^{-12}$, respectively. They can evolve as porosity changes (see Equation 2).

The results show that for both M30FA and M50 the numerical predictions of the total chloride concentration, expressed in % by mass of concrete, are close to the experimental data except for the first centimeter where other phenomena are not taken into account in the simulation such as wetting-drying cycles or competition between hydration and drying at early age. The difference in results also underlines that the two concretes behave very dissimilar. For M50 the contribution of chlorides physically adsorbed on C-S-H for M50 is much more important. In contrast, chemically bound chlorides incorporated in Friedel's and Kuzel's salt precipitation are less. These results can be explained by the initial hydrated mineral composition. The adopted modelling procedure for hydration does not predict any monosulfate for M50 (nor monocarbonate) which is the most important mineral that leads to the formation of Friedel's and Kuzel's salt (see Table 4). Chloride adsorption on C-S-H will then occur to a lesser extent as was already concluded in another study [51].

Although for the two concretes studied porosity values are very close to each other (see Table 2), chloride ingress is found to be faster in concrete M50 as can be seen in Figures 3 and 4 where for the two concretes the predicted generation of mineral as a function of depth after 19 year marine exposure are shown. The precipitation/dissolution front is then deeper and leads to a decrease of the pH value in the outer first centimeter due to leaching (see also Figure 5). The decrease of the bound chloride concentration is clear and emphasizes the fact that, even in saturated conditions, a profile with a "peak" at some distance from the concrete surface can also be observed as suggested by other studies [53, 68], in contrast to others, e.g. Ref. [69]. These results are analyzed in more detail in a recent paper [67]. In particular, the study shows that the model is able to numerically predict numerical profiles that are close to experimental data as well as to qualitatively estimate chemical and mineral zonation (magnesium, sulfur and chloride-rich zones) as observed in experiments.

4.2. Protective layer component dissolution

The simulations have been performed for a long time of exposure (50 years) considering a rebar depth relatively close to the concrete surface (3 cm) in order to assure that conditions conducive to corrosion initiation would be achieved. Of course, according to the standards for such a marine condition the cover depth should be more than 5 cm but this choice ensures a reduced calculation time. Figure 5 shows the calculated profiles giving the concentration as a function of depth after 50 year-exposure for

Table 6. Chemical equilibrium reactions, solubility products and kinetics parameters (specific surface $A_S[m^2.g^{-1}]$ and dissolution rate $k[mol.m^{-2}.s^{-1}]$) of the oxides and hydroxides present in the protective layer of the steel and the concrete mineral species.

Reaction	LogK	A_s	k	Ref.
C-S-H 1.6 $+6.4H^+ = 3.2Ca^{2+} + 2H_4SiO_4 + 2.6128H_2O$	55.94	41	2.75×10^{-12}	[59]
C-S-H 1.1 $+4.4H^+ = 2.2Ca^{2+} + 2H_4SiO_4 + 0.7491H_2O$	33.72	41	2.75×10^{-12}	[59]
Monosulfate $+12H^+ = 2Al^{3+} + 4Ca^{2+} + SO_4{}^{2-} + 18H_2O$	73.06	5.7	6.76×10^{-12}	[59]
Ettringite $+12H^+ = 2Al^{3+} + 6Ca^{2+} + 3SO_4{}^{2-} + 38H_2O$	56.96	9.8	7.08×10^{-13}	[59]
Hydrotalcite $+14H^+ = 2Al^{3+} + 4Mg^{2+} + 17H_2O$	73.73	9.8	10^{-9}	[59]
Portlandite $+2H^+ = Ca^{2+} + 2H_2O$	22.81	16.5	2.24×10^{-8}	[59]
Monocarbonate $+13H^+ = 2Al^{3+} + HCO_3{}^- + 4Ca^{2+} + 16.68H_2O$	80.54	5.7	6.76×10^{-12}	[59]
C3AH6 $+12H^+ = 2Al^{3+} + 3Ca^{2+} + 12H_2O$	80.32	16.5	2.24×10^{-10}	[59]
C3FS1.34H3.32 $+10H^+ + 5.64H_2O = 3Ca^{2+} + 2Fe^{2+} + 0.5O_2(aq) + 1.34H_4SiO_4$	42.76	9.8	7.08×10^{-13}	Deduced
Gypsum $= Ca^{2+} + SO_4{}^{2-} + 2H_2O$	−4.61	9.8	1.6×10^{-3}	[59]
Brucite $+2H^+ = Mg^{2+} + 2H_2O$	17.11	9.8	5.754×10^{-9}	[59]
Calcite $+H^+ = HCO_3{}^- + Ca^{2+}$	1.85	9.8	1.55×10^{-6}	[59]
Friedel's salt $+12H^+ = 2Al^{3+} + 4Ca^{2+} + 2Cl^- + 16H_2O$	74.92	5.7	6.76×10^{-12}	[59]
Kuzel's salt $+12.0000H^+ = 2Al^{3+} + 4Ca^{2+} + Cl^- + 0.5SO_4{}^{2-} + 18H_2O$	73.24	16.5	2.24×10^{-11}	Deduced
Lepidocrocite $+2H^+ = 0.25O_2(aq) + Fe^{2+} + 1.5H_2O$	–6.64	78	4.6×10^{-9}	[59]
Maghemite $+4H^+ = 0.5O_2(aq) + 2Fe^{2+} + 2H_2O$	–14.14	159.7?	1.15×10^{-8}	[59]
Goethite $+2H^+ = 0.25O_2(aq) + Fe^{2+} + 1.5H_2O$	–8.13	159.7	1.15×10^{-8}	[59]
Hematite $+4H^+ = 0.5O_2(aq) + 2Fe^{2+} + 2H_2O$	–17.03	159.7	2.51×10^{-15}	[59]
Magnetite $+6H^+ = 0.5O_2(aq) + 3Fe^{2+} + 3H_2O$	–6.62	231.5	1.66×10^{-11}	[59]
Akaganetite $+2.7H^+ = Fe^{2+} + 2.7H_2O + 0.3Cl^-$	–11.83	228	4.6×10^{-9}	Deduced
Reaction supposed to be instantaneous by lack of data				
Greenrust (Cl) $+7H^+ = Cl^- + 4Fe^{2+} + 0.25O_2(aq) + 7.5H_2O$	23.82			[59]
Greenrust (OH) $+6H^+ = 0.5O_2(aq) + 3Fe^{2+} + 5H_2O$	0.19			[59]
Greenrust (CO_3) $+11H^+ = HCO_3{}^- + 6Fe^{2+} + 0.5O_2(aq) + 13H_2O$	28.34			[59]
Greenrust (SO_3) $+14H^+ = 8Fe^{2+} + SO_4{}^{2-} + 19H_2O$	89.15			[59]
Greenrust (SO_4) $+10H^+ = 6Fe^{2+} + SO_4{}^{2-} + 0.5O_2(aq) + 13H_2O$	20.50			[59]

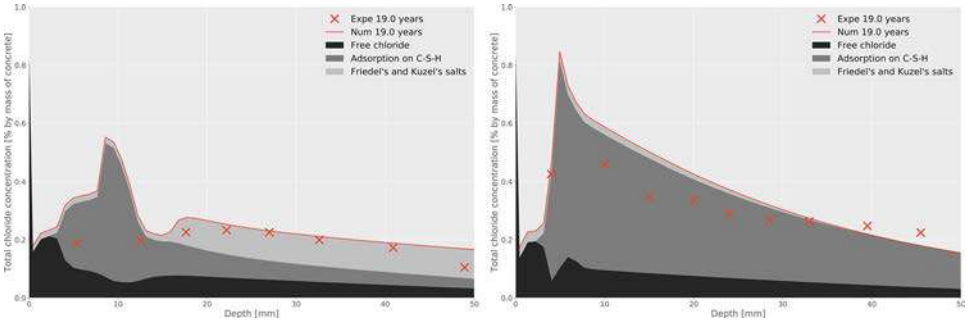

Figure 2. Comparison between experimental data and numerical results on total chloride concentration profile for M30FA (left) and M50 (right) [% by mass of concrete] after 19 year-exposure. Numerical total chloride is the sum of free chloride, chloride adsorbed on C-S-H and chloride that have reacted to form Friedel's and Kuzel's salts.

total chloride, free chloride and $[Cl^-]/[OH^-]$ ratio for the two concretes. These profiles are compared to commonly used (deterministic) chloride concentration threshold values: 0.4% by weight of binder for total chloride (equivalent to 2.75% and 2.1% by weight of concrete for M30FA and M50, respectively), $0.14mol.l^{-1}$ for free chloride and 0.6 for $[Cl^-]/[OH^-]$. In all cases, the threshold values are exceeded and corrosion initiation should thus have occurred.

Figure 6 shows the evolution of the components of the protective layer in concrete as a function of time resulting from continuous exposure to seawater. This figure also shows Fe-hydroxides susceptible to precipitate such as akaganeite which confirms experimental observation at steel-concrete interface [70]. The predicted results indicate that after several years of exposure the hydroxides (maghemite and lepidocrocite, known to be less stable than goethite, hematite or magnetite [43]) may totally dissolve whatever the the composition of the cement used in the concrete; both are converted into akaganeite. Another interesting result is the fact that in the specimen after 19 years of continuous marine exposure no precipitation of green rusts is observed (the different forms of green rust are not presented in Figure 6 because of the logarithm scale). These predicted results also indicate that the denser part of the protective layer composed of hematite, magnetite and goethite are thermodynamically very stable.

For the two concretes these precipitation/dissolution phenomena are accompanied by a mass increase of the protective layer as a function of time (see Figure 7). Such a result is confirmed by an experimental study which measures mass increase prior to pitting corrosion whereas some

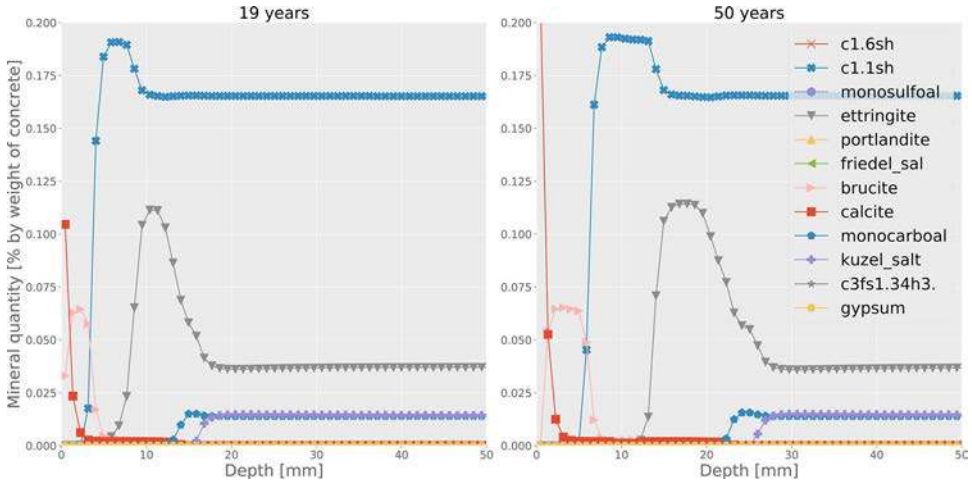

Figure 3. Dissolution and precipitation of mineral species resulting from exposure to seawater for M30FA [% by mass of concrete] after 19 and 50 year-exposure.

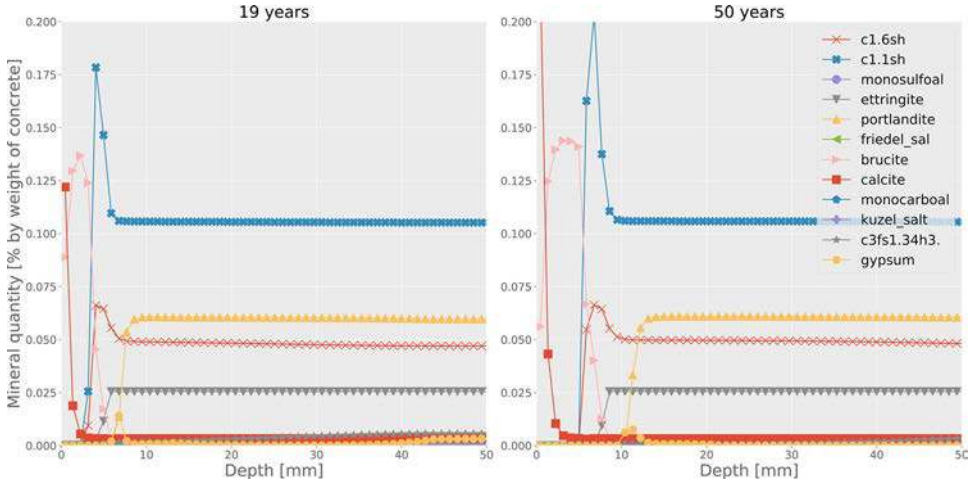

Figure 4. Dissolution and precipitation of mineral species resulting from exposure to seawater for M50 [% by mass of concrete] after 19 and 50 year-exposure.

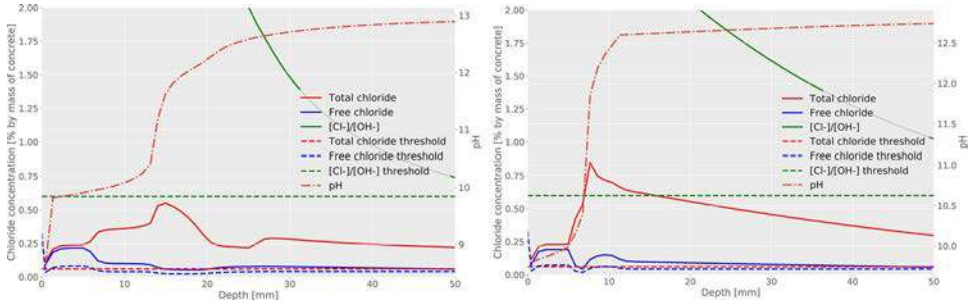

Figure 5. Comparison between chloride threshold values (total chloride, free chloride and $[Cl^-]/[OH^-]$ ratio) and chloride profiles for M30FA (left) and M50 (right) after 50 year-exposure.

measured electrochemical parameters measured (OCP, impedance and phase angle) indicate stable passivity [15], suggesting that passivity is mainly controlled by the inner layer of oxides. In the present study, the increase in mass is exclusively due to precipitation of akaganeite. The main difference in behavior between the two concretes is the precipitation rate of akaganeite which is faster for M30FA due to a greater decrease of the pH value close to the exposed surface (see Figure 5).

5. Discussion

This work confirms that other phenomena than dissolution need to occur in order to break down the protective layer whatever the time of exposure. One mechanism in which dissolution of Fe-hydroxides may lead to corrosion initiation is given by Fe-hydroxides which are in direct physical contact with the "healthy" steel. Such a mechanism is possible if cracks appear in the inner denser part of the protective layer and if hydroxides precipitate in the cracks.

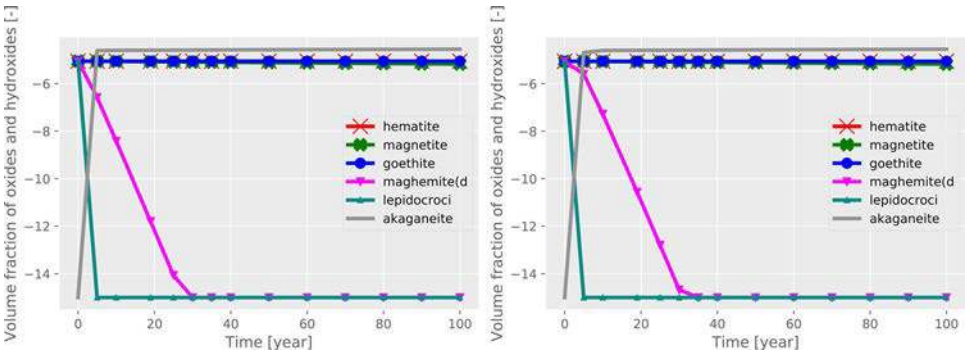

Figure 6. Protective layer component evolution (logarithmic scale) as a function of time for M30FA (left) and M50 (right).

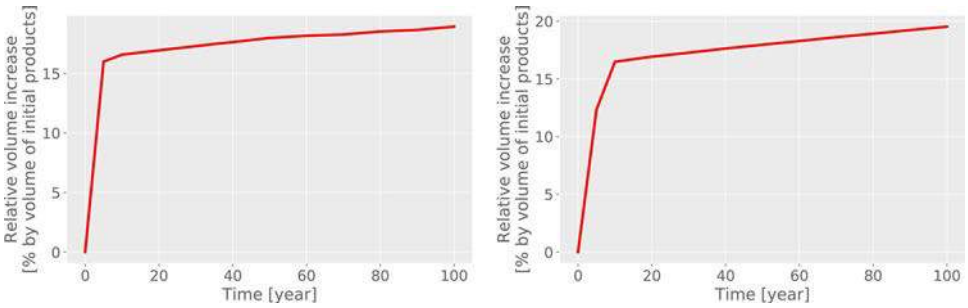

Figure 7. Percentage of relative volume increase of corrosion products as a function of time for M30FA (left) and M50 (right).

This can be observed when the denser part of the protective layer cracks after factory manufacture process and when lepidocrocite precipitates in this cracks due to atmospheric corrosion prior to casting.

When cracks or micro-cracks appear during handling prior to embedment in concrete (e.g. transport, storage or embedment setup), different corrosion products can be observed depending on the rebar conditions of exposure. Carbon steel exposed to natural weathering (atmophere) implies the precipitation of lepidocrocite, mainly, and goethite and magnetite but in lower concentrations [71]. In that case, depassivation can occur as is indicated in Figure 6. In particular, lepidocrocite can dissolve and akaganeite can precipitate, the latter one being observe during corrosion in the inner part of the corrosion layer, near the metal-oxide interface (Ref. [72] to cite one of many works). Figure 6 shows also the time for which the dissolution of lepidocrocite is completed. This time may be identified to an induction period before corrosion starts as suggested by other authors [15].

When for steel embedded in concrete cracks appear in the protective layer in concrete, phenomena are quite different and conclusions are difficult to drawn because experimental data on depassivation conditions in concrete are missing. Many electrochemical studies have been performed with steel immersed in saturated calcium hydroxide solutions [73–76]. Most of the corrosion products found are magnetite [31], however the use of saturated calcium hydroxides solution does not seem to be relevant to investigate the formation and dissolution of the passive films as the pore solutions contains a variety of ions depending on the binder type, e.g. sodium, potassium, hydroxides and sulfate ions [13–15, 77]. Gui and Devine [77] have shown by observations with Raman spectroscopy that the structure and nature of the passive film are influenced by the sulfate anions contained in the pore solution. Veleva *et al.* [13, 78], Montemor *et al.* [79] and Ghods *et al.* [14] demonstrated by electrochemical measurements and SEM analysis or X ray photoelectron spectroscopy the dissimilarities between films grown in different solutions. Ghods [14] studied the quality of the passive film also with steel immersed in saturated calcium hydroxide solutions containing different amounts of $NaOH$, KOH and $Ca(SO_4)$ for simulating a concrete pore environment: the various ion concentrations imply differences during the formation and dissolution of oxides and hydroxides. In particular it has been observed by electrochemical measurement that sulfate anions have a negative effect on the protective properties of the passive layer. The SEM observations have identified cracks and voids over the surface of the rebar showing a distribution dependent on the amount of ions. Nevertheless, experimental data on depassivation conditions in concrete are missing due to the difficulty to observe such a phenomenon and further study are thus required.

6. Conclusions

In this study the critical chloride threshold concentration leading to initiation of reinforcement corrosion in concrete exposed to seawater has been put under discussion. Indeed, such a concept assumes that degradation of the protective layer is independent of geometrical factors related to protective layer thickness that aggressive ionic species should pass through. Indeed, in such a case and if chloride ions are able to pass through the protective layer, the chloride concentration in the vicinity of the protective layer should evolve during ingress of chloride through

the protective layer leading to significant scatter in critical chloride concentration when first signs of corrosion are observed. This concept also assumes that the degradation will be independent of cracks in the protective layer which could occur at any time. Cracking would also lead to scatter in the critical chloride concentration. The concept of a critical chloride concentration is then related to the dissolution conditions of the external protective layer components composed of maghemite and lepidocrocite and the internal, denser part of the protective layer composed of magnetite, goethite, and hematite.

A reactive transport model previously validated for concretes exposed to chloride and seawater has been used in order to examine the conditions for the dissolution of the Fe-oxides and hydroxides present in the protective layer covering a steel rebar. This model includes chemical reactions taking into account the kinetics of most of concrete mineral species [57, 60] (C-S-H1.6, C-S-H1.1, Monosulfate, Ettringite, Portlandite, Monocarbonate, $C_3FS_{1.34}H_{3.32}$, Gypsum) and mineral species that may precipitate (Brucite, Calcite, Friedel's, and Kuzel's salt). It takes also into account adsorption of ionic species on C-S-H.

The results show that in the case of the two types of concretes selected:

- All Fe-oxides present in the inner part of the protective layer are thermodynamically stable even after 50 years of exposure;
- Lepidocrocite and maghemite are able to dissolve in the presence of seawater in the case of saturated concretes which leads to akaganeite precipitation;
- No green rust precipitates whereas this corrosion product can be observed on steel immersed in seawater [47].

These findings imply that, for the two studied concretes, the degradation process of the protective layer, implying dissolution of its two layers (oxides and hydroxides), cannot be explained by the dissolution of the Fe-hydroxides alone neither by the chemistry of the concrete pore solution in the vicinity of the steel/concrete interface. Other phenomena such as diffusion of aggressive agents through the protective layer or diffusion of Fe^{2+}-ions from the reinforcement as well as cracks in the protective layer are necessary. In this case, the thickness of the protective layer or even its nature and mechanical history are essential elements to predict the conditions for its degradation. Then, the concept of critical chloride thresholds from concentration measurements in concrete seems not to be sufficient since the degradation depends on geometrical factors as well as mechanical stress which leads to significant scatter in the critical chloride concentration.

Of course, prediction of time to corrosion remains and is still a subject of debate in the literature. Thus, the different scenarios considered in the literature review of the present paper should be treated more deeply (presence of defects, diffusion through the protective layer, electrochemical migration …) in order to try to express time to corrosion as a function of protective layer thickness, manufacturing process, mechanical history, electro-chemical conditions and not only as a function of chemical dissolution.

Disclosure statement

No potential conflict of interest was reported by the authors.

ORCID

Anthony Soive http://orcid.org/0000-0002-2368-6848
Stéphanie Bonnet http://orcid.org/0000-0003-0027-344X

References

[1] Angst U, Elsener B, Larsen CK, et al. Critical chloride content in reinforced concrete—a review. Cem Concr Res. 2009;39(12):1122–1138.
[2] Cao Y, Gehlen C, Angst U, et al. Critical chloride content in reinforced concrete—an updated review considering Chinese experience. Cem Concr Res. 2019;117:58–68.
[3] American Society for Testing Materials, ASTM C-1152. Standard test method for acid-soluble chloride in mortar and concrete.
[4] Andrade C, Castellote M. Testing and modelling chloride penetration in concrete: analysis of total chloride content in concrete. Mater Struct. 2002;35:583–585.
[5] Alonso C, Andrade C, Castellote M, et al. Chloride threshold values to depassivate reinforcing bars embedded in a standardized OPC mortar. Cem Concr Res. 2000;30(7):1047–1055.
[6] Hausmann DA. Steel corrosion in concrete. How does it occur? Mater Protect. 1967;6:19–23.
[7] Gouda VK. Corrosion and corrosion inhibition of reinforcing steel. I. Immersed in alkaline solutions. Br Corros J. 1970;5(5):198–203.
[8] Glass GK, Buenfeld NR. The presentation of the chloride threshold level for corrosion of steel in concrete. Corros Sci. 1997;39(5):1001–1013.
[9] Mammoliti LT, Brown LC, Hansson CM, et al. The influence of surface finish of reinforcing steel and pH of the test solution on the chloride threshold concentration for corrosion initiation in synthetic pore solutions. Cem Concr Res. 1996;26(4):545–550.
[10] Li L, Sagüés AA. Chloride corrosion threshold of reinforcing steel in alkaline solutions-open-circuit immersion tests. Corrosion. 2001;57(1):19–28.
[11] Pillai RG, Trejo D. Surface condition effects on critical chloride threshold of steel reinforcement. ACI Mater J. 2005;102:103–109.
[12] Ghods P, Isgor OB, Brown JR, et al. XPS depth profiling study on the passive oxide film of carbon steel in saturated calcium hydroxide solution and the effect of chloride on the film properties. Appl Surf Sci. 2011;257(10):4669–4677.
[13] Veleva L, Alpuche-Aviles MA, Graves-Brook MK, et al. Comparative cyclic voltammetry and surface analysis of passive films grown on stainless steel 316 in concrete pore model solutions. Electroanal Chem. 2002;537(1-2):85–93.
[14] Ghods P, Isgor OB, Mcrae G, et al. The effect of concrete pore solution composition on the quality of passive oxide films on black steel reinforcement. Cem Concr Compos. 2009;31(1):2–11.

[15] Gunay HB, Isgor B, Ghods P. Kinetics of passivation and chloride-induced depassivation of iron in simulated concrete pore solutions using electrochemical quartz crystal. Corrosion. 2015;71(5):615–627.
[16] Alhozaimy A, Hussain RR, Al-Negheimish A. Significance of oxygen concentration on the quality of passive film formation for steel reinforced concrete structures during the initial curing of concrete. Cem Concr Compos. 2016;65:171–176.
[17] Ann KY, Song H-W. Chloride threshold level for corrosion of steel in concrete. Corros Sci. 2007;49(11): 4113–4133.
[18] Wedding PA, Diamond S. Chloride concentrations in concrete pore solutions resulting from calcium and sodium chloride admixtures. Cement Concr Aggr. 1986; 8(2):97–102.
[19] Moreno M, Morris W, Alvarez MG, et al. Corrosion of reinforcing steel in simulated concrete pore solutions: effect of carbonation and chloride content. Corros Sci. 2004;46(11):2681–2699.
[20] Yu L, François R, Dang VH, et al. Development of chloride-induced corrosion in pre-cracked RC beams under sustained loading: effect of load-induced cracks, concrete cover, and exposure conditions. Cem Concr Res. 2015;67:246–258..
[21] Kolotyrkin YJ. Pitting corrosion of metals. Corrosion. 1963;19(8):261–268.
[22] Dabosi F, Baroux B. Corrosion localisée. EDP Sciences Edition; 1994.
[23] Hoar TP, Mears DC, Rothwell GP. The relationships between anodic passivity, brightening and pitting. Corros Sci. 1965;5(4):279–289.
[24] Vetter KJ, Strehblow HH. Entstehung und gestalt von korrosionslöchern bei lochfraßan eisen und theoretische folgerungen zur lochfraßkorrosion. Berichte Bunsengesellschaft Phys Chem. 1970;1024–1035.
[25] Strehblow H-H. Nucleation and repassivation of corrosion pits for pitting on iron and nickel. Mater Corros. 1976;27(11):792–799.
[26] Kenny A, Katz A. Steel-concrete interface influence on chloride threshold for corrosion—empirical reinforcement to theory. Constr Build Mater. 2020;244:118376.. https://www.sciencedirect.com/science/article/pii/S0950061820303810
[27] Poursaee A. Corrosion of steel bars in saturated $Ca(OH)_2$ and concrete pore solution. Concr Res Lett. 2010;1:90–97.
[28] Ghods P, Isgor OB, Carpenter GJC, et al. Nano-scale study of passive films and chloride-induced depassivation of carbon steel rebar in simulated concrete pore solutions using FIB/TEM. Cem Concr Res. 2013;47(0): 55–68.
[29] Sanchez M, Gregori J, Alonso C, et al. Electrochemical impedance spectroscopy for studying passive layers on steel rebars immersed in alkaline solutions simulating concrete pores. Electrochim Acta. 2007;52(27): 7634–7641.
[30] Pourbaix M. Atlas d'équilibres électrochimiques à $25^{\circ}C$. Gauthier-Villars et CEBELCOR, 1963.
[31] Joiret S, Keddam M, Novoa XR, et al. Use of EIS, ring-disk electrode, EQCM and raman spectroscopy to study the film of oxides formed on iron in 1 M NaOH. Cement Concr Compos. 2002;24(1):7–15.
[32] Sanchez M, Gregori J, Alonso MC, et al. Anodic growth of passive layers on steel rebars in an alkaline medium simulating the concrete pores. Electrochim Acta. 2006;52(1):47–53.
[33] Sanchez-Moreno M, Takenouti H, Garcia-Janero JJ, et al. A theoretical approach of impedance spectroscopy during the passivation of steel in alkaline media. Electrochim Acta. 2009;54(28):7222–7226.
[34] Ghods P, Isgor OB, Bensebaa F, et al. Angle-resolved XPS study of carbon steel passivity and chloride-induced depassivation in simulated concrete pore solution. Corros Sci. 2012;58:159–167.
[35] Gunay HB, Ghods P, Isgor OB, et al. Characterization of atomic structure of oxide films on carbon steel in simulated concrete pore solutions using EELS. Appl Surf Sci. 2013;274(0):195–202.
[36] Suda K, Misra S, Motohashi K. Corrosion products of reinforcing bars embedded in concrete. Corros Sci. 1993;35(5-8):1543–1549.
[37] Noda K, Tsuru T, Haruyama S. The impedance characteristics of passive films on iron. Corros Sci. 1990; 31(0):673–678.
[38] Pan T, Van Duin ACT. Passivation of steel surface: an atomistic modeling approach aided with X-ray analyses. Mater Lett. 2011;65(21-22):3223–3226.
[39] Zakroczymski T, Fan C-J, Szklarska-Smialowska Z. Kinetics and mechanism of passive film formation on iron in 0.05M NaOH. J Electrochem Soc. 1985; 132(12):2862–2867.
[40] Haupt S, Strehblow HH. Corrosion, layer formation, and oxide reduction of passive iron in alkaline solution: a combined electrochemical and surface analytical study. Langmuir. 1987;3(6):873–885.
[41] Miserque F, Huet B, Azou G, et al. X-ray photoelectron spectroscopy and electrochemical studies of mild steel FeE500 passivation in concrete simulated water. J Phys IV France. 2006;136:89–97.
[42] Sagoe-Crentsil KK, Glasser FP. Green rust, iron solubility and the role of chloride in the corrosion of steel at high pH. Cem Concr Res. 1993;23(4):785–791.
[43] Cornell R, Schwertmann U. The iron oxides: structure, properties, reactions, occurrences and uses. Wiley-VCH Verlag GmbH & Co. KGaA, 2003.
[44] Asami K, Kikuchi M. In-depth distribution of rusts on a plain carbon steel and weathering steels exposed to coastal industrial atmosphere for 17 years. Corros Sci. 2003;45(11):2671–2688.
[45] Morcillo M, Alcantara J, Diaz I, et al. Marine atmospheric corrosion of carbon steels. REVMETAL. 2015; 51(2):e045.
[46] Abdelmoula M, Refait P, Drissi S, et al. Conversion electron mössbauer spectroscopy and x-ray diffraction studies of the formation of carbonate-containing green rust one by corrosion of metallic iron in $NaHCO_3$ and ($NaHCO_3$ + NaCl) solutions. Corros Sci. 1996;38(4): 623–633. https://www.sciencedirect.com/science/article/pii/0010938X9500153B
[47] Refait P, Abdelmoula M, Génin J-MR. Mechanisms of formation and structure of green rust one in aqueous corrosion of iron in the presence of chlorides ions. Corros Sci. 1998;40(9):1547–1560.
[48] Hansen HCB. Composition, stabilization, and light absorption of Fe(II)Fe(III) hydroxy-carbonate ('green rust'). Clay Miner. 1989;24(4):663–669.
[49] Abdelmoula M, Trolard F, Bourrié G, et al. Evidence for the Fe(II)-Fe(III) green rust" fougerite" mineral occurrence in a hydromorphic soil and its transformation with depth. Hyperfine Interact. 1998;112(1/4):235–238. https://doi.org/10.1023/A:1010802508927
[50] Tran V-Q, Soive A, Baroghel-Bouny V. Modelisation of chloride reactive transport in concrete including thermodynamic equilibrium, kinetic control and surface complexation. Cem Concr Res. 2018;110:70–85.
[51] Tran V-Q, Soive A, Bonnet S, et al. A numerical model including thermodynamic equilibrium, kinetic control and surface complexation in order to explain cation type effect on chloride binding capability of concrete. Constr Build Mater. 2018;191:608–618.

[52] Soive A, Tran V-Q. External sulfate attack of cementitious materials: new insights gained through numerical modeling including dissolution/precipitation kinetics and surface complexation. Cem Concr Compos. 2017; 83:263–272.
[53] Soive A, Tran V-Q, Baroghel-Bouny V. Requirements and possible simplifications for multi-ionic transport models—case of concrete subjected to wetting-drying cycles in marine environment. Constr Build Mater. 2018;164:799–808.
[54] Lasaga AC, Soler JM, Ganor J, et al. Chemical weathering rate laws and global geochemical cycles. Geochim Cosmochim Acta. 1994;58(10):2361–2386.
[55] Baroghel-Bouny V, Dierkens M, Wang X, et al. Ageing and durability of concrete in lab and in field conditions: investigation of chloride penetration. J Sustain Cement Based Mater. 2013;2(2):67–110.
[56] Lavergne F, Ben Fraj A, Bayane I, et al. Estimating the mechanical properties of hydrating blended cementitious materials: an investigation based on micromechanics. Cem Concr Res. 2018;104:37–60.
[57] Dilnesa BZ, Lothenbach B, Renaudin G, et al. Synthesis and characterization of hydrogarnet $Ca_3(Al_xFe_{1-x})_2(SiO_4)_y\ (OH)_{4(3-y)}$. Cem Concr Res. 2014;59:96–111.
[58] Xu T, Spycher N, Sonnenthal E. TOUGHREACT user's guide: a simulation program for non-isothermal multiphase reactive transport in variably saturated geologic media, version 2.0, 2012.
[59] Blanc P, Lassin A, Piantone P, et al. Thermoddem: a geochemical database focused on low temperature water/rock interactions and waste materials. Appl Geochem. 2012;27(10):2107–2116.
[60] Lothenbach B, Kulik DA, Matschei T, et al. Cemdata18: a chemical thermodynamic database for hydrated Portland cements and alkali-activated materials. Cem Concr Res. 2019;115:472–506.
[61] Diakonov I. Etude expérimentale de la complexation de l'aluminium avec l'ion sodium et de la spéciation du gallium et du fer (III) dans les solutions naturelles [PhD thesis]. Toulouse (France): Université Paul Sabatier; 1995.
[62] Cox JD, Wagman DD, Medvedev VA. CODATA key values for thermodynamics. New York (NY): Hemisphere Publishing Corp; 1989.
[63] Shock EL, Sassani DC, Willis M, et al. Inorganic species in geologic fluids: correlations among standard molal thermodynamic properties of aqueous ions and hydroxide complexes. Geochim Cosmochim Acta. 1997;61(5):907–950.
[64] Balonis M, Lothenbach B, Saout GL, et al. Impact of chloride on the mineralogy of hydrated Portland cement systems. Cem Concr Res. 2010;40(7):1009–1022.
[65] Tran V-Q. Contribution à la compréhension des mécanismes de dépassivation des armatures d'un béton exposé à l'eau de mer: théorie et modélisation thermochimique [PhD thesis]. Nantes (France): Ecole Centrale de Nantes; 2016.
[66] Snow CL, Smith SJ, Lang BE, et al. Heat capacity studies of the iron oxyhydroxides akaganéite (β-FeOOH) and lepidocrocite (γ-FeOOH). J Chem Thermodyn. 2011;43(2):190–199.
[67] Soive A, Baroghel-Bouny V, Lavergne F. Durability of concretes exposed to seawater and wetting drying cycles in field conditions during 20 years (accepted). In: 15th International Conference on Durability of Building Materials and Components, Barcelona, 2020.
[68] Othmen I, Bonnet S, Schoefs F. Statistical investigation of different analysis methods for chloride profiles within a real structure in a marine environment. Ocean Eng. 2018;157:96–107.
[69] Medeiros-Junior R, Lima M, Brito P, et al. Chloride penetration into concrete in an offshore platform-analysis of exposure conditions. Ocean Eng. 2015;103: 78–87.
[70] Serdar M, Meral C, Kunz M, et al. Spatial distribution of crystalline corrosion products formed during corrosion of stainless steel in concrete. Cem Concr Res. 2015;71:93–105.
[71] Antunes RA, Ichikawa RU, Martinez LG, et al. Characterization of corrosion products on carbon steel exposed to natural weathering and to accelerated corrosion tests. Int J Corros. 9.
[72] Neff D, Dillmann P, Bellot-Gurlet L, et al. Corrosion of iron archaeological artefacts in soil: characterisation of the corrosion system. Corros Sci . 2005;47(2): 515–535.
[73] Blanco G, Bautista A, Takenouti H. EIS study of passivation of austenitic and duplex stainless steels reinforcements in simulated pore solutions. Cem Concr Compos. 2006;28(3):212–219.
[74] Saremi M, Mahallati E. A study on chloride-induced depassivation of mild steel in simulated concrete pore solution. Cem Concr Res. 2002;32(12):1915–1921.
[75] Elshami AA, Bonnet S, Khelidj A, et al. Novel anticorrosive zinc phosphate coating for corrosion prevention of reinforced concrete. Eur J Environ Civil Eng. 2017; 21(5):572–593.
[76] Elshami A, Bonnet S, Khelidj A, et al. Effectiveness of corrosion inhibitors in simulated concrete pore solution. Eur J Environ Civil Eng. 2020;24(13):2130–2150.
[77] Gui J, Devine TM. The influence of sulfate ions on the surface enhanced Raman spectra of passive films formed on iron. Corros Sci. 1994;36(3):441–462.
[78] Veleva L, Cebada MC. Marine corrosion in tropical environments. West conshohocken (PA): ASTM Edition; 2000.
[79] Montemor MF, Simões AM, Ferreira MG. Analytical characterization of the passive film formed on steel in solutions simulating the concrete interstitial electrolyte. Corrosion. 1998;54(5):347–353.